Inorganics **2015**, *3*, 554-572; doi:10.3390/inorganics3040554

OPEN ACCESS

inorganics

ISSN 2304-6740

www.mdpi.com/journal/inorganics

Article

Magnetic and Photo-Physical Properties of Lanthanide Dinuclear Complexes Involving the 4,5-Bis(2-Pyridyl-*N*-Oxidemethylthio)-4′,5′-Dicarboxylic Acid-Tetrathiafulvalene-, Dimethyl Ester Ligand

Fabrice Pointillart [1,*], Saskia Speed [1], Bertrand Lefeuvre [1], François Riobé [2], Stéphane Golhen [1], Boris Le Guennic [1], Olivier Cador [1], Olivier Maury [2] and Lahcène Ouahab [1]

[1] Institut des Sciences Chimiques de Rennes UMR 6226 CNRS-UR1, Université de Rennes 1, 35042 Rennes Cedex, France; E-Mails: saskia.speed@univ-rennes1.fr (S.S.); bertrand.lefeuvre@univ-rennes1.fr (B.L.); stephane.golhen@univ-rennes1.fr (S.G.); boris.leguennic@univ-rennes1.fr (B.L.G.); olivier.cador@univ-rennes1.fr (O.C.); lahcene.ouahab@univ-rennes1.fr (L.O.)

[2] Laboratoire de Chimie de l'ENS-LYON-UMR 5182, 46 Allée d'Italie, 69364 Lyon Cedex 07, France; E-Mails: francois.riobe@ens-lyon.fr (F.R.); olivier.maury@ens-lyon.fr (O.M.)

* Author to whom correspondence should be addressed; E-Mail: fabrice.pointillart@univ-rennes1.fr; Tel.: +33-2-23-23-57-62; Fax: +33-2-23-23-68-40.

Academic Editors: Stephen Mansell and Steve Liddle

Received: 15 October 2015 / Accepted: 23 November 2015 / Published: 3 December 2015

Abstract: The reaction between the 4,5-bis(2-pyridyl-*N*-oxidemethylthio)-4′,5′-dicarboxylic acid-tetrathiafulvalene-, dimethyl ester ligand (**L**) and the metallo-precursors $Ln(hfac)_3 \cdot 2H_2O$ leads to the formation of two dinuclear complexes of formula $[Ln_2(hfac)_6(\mathbf{L})] \cdot (CH_2Cl_2) \cdot (C_6H_{14})_{0.5}$ (Ln^{III} = Dy^{III} (**1**) and Yb^{III} (**2**)). The X-ray structure reveals a quite regular square anti-prism symmetry for the coordination sphere of the lanthanide ion. UV-visible absorption properties have been experimentally measured and rationalized by TD-DFT calculations. The functionalization of the tetrathiafulvalene (TTF) core by two methyl ester moieties induces the appearance of an additional absorption band in the lowest-energy region of the spectrum. The latter has been identified as a HOMO (Highest Occupied Molecular Orbital)→LUMO (Lowest Unoccupied Molecular Orbital) Intra-Ligand Charge Transfer (ILCT) transition in which the HOMO and LUMO are centred on the TTF and methyl ester groups, respectively. Irradiation at 22,222 cm^{-1} of this ILCT band induces an efficient sensitization of the Yb^{III}-centred emission that can be correlated to the magnetic properties.

Keywords: lanthanides; tetrathiafulvalene; magnetism; photo-physics; TD-DFT calculations

1. Introduction

Since the discovery of the first mononuclear single molecule magnet (SMM) of lanthanide [1], f-elements have taken a preponderant place in the elaboration of coordination complexes in the field of molecular magnetism [2–11]. Lanthanide ions indeed have several advantages, such as strong single-ion anisotropy and large magnetic moment [12,13]. Recently, actinides have started to contribute to the development of new SMMs due to their strong magnetic anisotropy and larger exchange interactions coming from the more extended nature of the 5f orbitals [14–20]. On one hand, SMMs are molecular objects with potential applications in quantum computing, high-density memory data storage devices, and spintronics [21–29]. On the other hand, lanthanide ions are widely exploited for their specific luminescence which displays sharp f–f transitions ranging from the visible to the near infrared (NIR) region. Nevertheless, the very weak intensity of the f–f absorption bands (Laporte forbidden) [30] makes a direct excitation less straightforward, and consequently, lanthanide ions are usually coordinated to an organic ligand that strongly absorbs light in the UV-visible range. Thus, this organic ligand plays the role of organic chromophore for the sensitization of the lanthanide's luminescence through an antenna effect [31,32]. In addition to the interest of lanthanide ions in coordination chemistry, a main challenge that chemists face is to use organic ligands that induce various behaviours such as redox activity, emission, magnetism, chirality, *etc.*, and lead to multi-properties (functional) coordination complexes or SMMs [33–35]. In this context, a few years ago we started to combine lanthanide ions and tetrathiafulvalene (TTF)-based ligands which were used for their electron donating ability, redox activity and electronic conductivity [36–44]. We have already demonstrated that such ligands are suitable to obtain SMMs [45–51] and to sensitize lanthanide luminescence [52–56]. Previously, we associated the $Ln(hfac)_3 \cdot 2H_2O$ ($hfac^-$ = 1,1,1,5,5,5-hexafluoroacetyacetonate) metallo-precursors with the (4,5-bis(2-pyridyl-*N*-oxidemethylthio)-4′,5′)-ethylenedithiotetrathiafulvene, -methyldithiotetrathiafulvene [57], or -4′,5′-ethylendioxotetrathiafulvalene ligands, leading to several dinuclear complexes [58].

In the present contribution we go one step forward, using the new 4,5-bis(2-pyridyl-*N*-oxidemethylthio)-4′,5′-dicarboxylic acid-tetrathiafulvalene-, dimethyl ester ligand (**L**). The coordination reactions of $Ln(hfac)_3 \cdot 2H_2O$ (Ln = Dy^{III} (**1**) and Yb^{III} (**2**)) with (**L**) are presented and the X-ray structure of $[Dy_2(hfac)_6(\mathbf{L})] \cdot (CH_2Cl_2) \cdot (C_6H_{14})_{0.5}$ is described. The photo-physical and magnetic properties of **1** and **2** are presented and discussed.

2. Results and Discussion

2.1. Synthesis

The target ligand **L** (Scheme 1) was prepared by deprotection of the thiol function of the 4,5-dicarboxylic acid-4′,5′-bis(2-cyanoethyl)thio)-tetrathiafulvalene-, dimethyl ester [59] with sodium methoxide or cesium hydroxide and then grafting of the 2-methylpyridine-1-oxide coordinating groups.

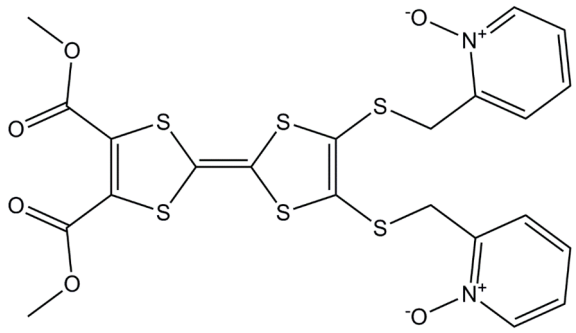

Scheme 1. Chemical structure of the new 4,5-bis(2-pyridyl-*N*-oxidemethylthio)-4′,5′-dicarboxylic acid-tetrathiafulvalene-, dimethyl ester ligand, **L**.

L can be described as a multiply functionalized ligand with two pyridine-*N*-oxide moieties that are suitable for the coordination of lanthanide ions, leading generally to the formation of dinuclear complexes on one side and two ester groups on the other side, whose electron-withdrawing character will monitor the ligand's electronic properties. These ester moieties could also be hydrolysed into carboxylate functions acting as additional coordinating sites [60].

*2.2. Crystal Structure of [$Dy_2(hfac)_6$(**L**)]·(CH_2Cl_2)·(C_6H_{14})$_{0.5}$ (**1**)*

Compound **1** crystallizes in the Pcab (No.61) orthorhombic space group (Tables 1 and 2). The asymmetric unit is composed of two Dy(hfac)$_3$ moieties, two **L** ligands and one dichloromethane molecule of crystallization. An ORTEP (Oak Ridge Thermal Ellipsoid Plot) view is depicted in Figure 1.

Table 1. X-ray crystallographic data for **1**.

Compounds	**$[Dy_2(hfac)_6(L)_2]\cdot(CH_2Cl_2)\cdot 0.5C_6H_{14}$ (1)**
Formula	$C_{78}H_{51}Cl_2Dy_2F_{36}N_4O_{24}S_{12}$
M/g·mol^{-1}	2892.84
Crystal system	Orthorhombic
Space group	Pcab (No.61)
Cell parameters	*a* = 17.3005(5) Å *b* = 34.2288(10) Å *c* = 37.6768(10) Å
Volume/Å^3	22,311.3(11)
Z	8
T/K	150 (2)
2θ range/°	2.16 ≤ 2θ ≤ 54.96
ρcalc/g·cm^{-3}	1.722
μ/mm^{-1}	1.728
Number of reflections	103,297
Independent reflections	25,452
Rint	0.0815
$Fo^2 > 2\sigma(Fo)^2$	13,844
Number of variables	1396
*R*1, w*R*2	0.0805, 0.2175

Table 2. Selected bond lengths (Å) for compound **1**.

Compounds	1
Dy1–O9	2.263(8)
Dy1–O10	2.324(6)
Dy1–O11	2.376(7)
Dy1–O12	2.347(7)
Dy1–O13	2.359(7)
Dy1–O14	2.366(7)
Dy1–O15	2.381(7)
Dy1–O16	2.380(8)
Dy2–O17	2.344(7)
Dy2–O18	2.264(7)
Dy2–O19	2.359(7)
Dy2–O20	2.361(8)
Dy2–O21	2.352(8)
Dy2–O22	2.326(8)
Dy2–O23	2.382(7)
Dy2–O24	2.394(8)

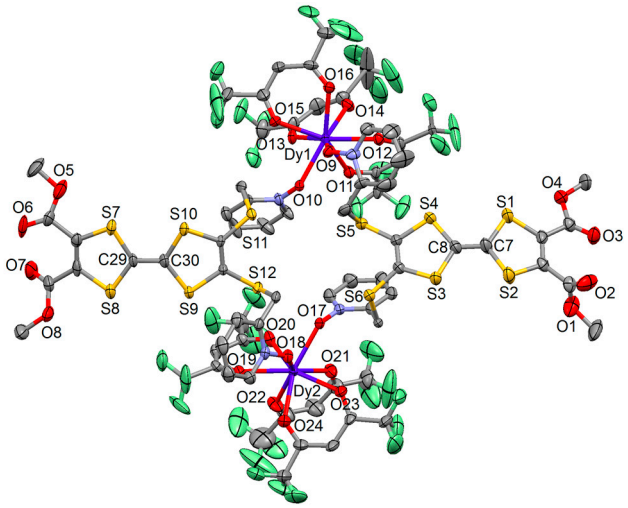

Figure 1. ORTEP view of **1** ($[Dy_2(hfac)_6(L)_2]\cdot(CH_2Cl_2)\cdot 0.5C_6H_{14}$). Thermal ellipsoids are drawn at 30% probability. Hydrogen atoms and solvent molecules of crystallization are omitted for clarity.

The X-ray structure reveals that two $Dy(hfac)_3$ moieties are bridged by two **L** ligands. The two water molecules of the starting metallo-precursor have been substituted by two pyridine-*N*-oxide groups. The Dy1 and Dy2 ions are surrounded by eight oxygen atoms that belong to three $hfac^-$ ligands and the two pyridine-*N*-oxide coordinating acceptors. The average Dy–O distances are equal to 2.350(7) and 2.348(8) Å for Dy1 and Dy2, respectively. The arrangement of the ligands leads to a square antiprism (D_{4d} symmetry) as coordination polyhedron for both dysprosium ions ($CShM_{SAPR-8} = 0.385$ for Dy1 and $CShM_{SAPR-8} = 0.396$ for Dy2). The distortion is visualized by continuous shape measures performed with SHAPE 2.1 [61]. The Dy coordination polyhedra in **1** are the most symmetrical of all the series of similar dinuclear complexes that we have already obtained [57,58].

The central C=C bonds of the TTF core are equal to 1.342(13) and 1.340(16) Å, which attests the neutral form of **L**. The ester functions play an important role in the cohesion of the crystal packing. While the ester groups involving O5–O8 are almost parallel, those involving O1–O4 are almost perpendicular, in order to optimize the intermolecular S···O short contacts.

The combination of the shortest S···S contacts (3.668 Å (S3···S3) and 3.889 Å (S3···S6)) and shortest S···O contacts (3.281 Å (S8···O1), 3.364 Å (S1···O5), and 3.493 Å (S3···O7)) leads to the formation of tetramers of donors (Figure 2). The shortest intra- and inter-molecular Dy–Dy distances are equal to 10.052 Å (Dy1···Dy2), 11.039 Å (Dy2···Dy2), and 11.340 Å (Dy1···Dy1).

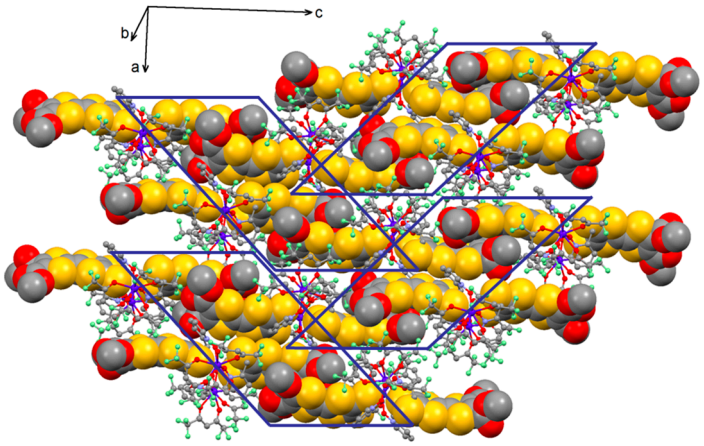

Figure 2. Crystal packing of **1** highlighting the formation of tetramers of **L** through short S···S and S···O contacts. Colour code: grey (C), red (O), orange (S), blue (D), green (F).

2.3. Electrochemical Properties

The redox properties of **L** and related complexes **1** and **2** ($[Yb_2(hfac)_6(\mathbf{L})_2]\cdot CH_2Cl_2\cdot(C_6H_{14})_{0.5}$) are investigated by cyclic voltammetry (Figure S1) and the values of the oxidation potentials are listed in Table 3.

Table 3. Oxidation potentials (V *vs.* saturated calomel electrode, nBu_4NPF_6, 0.1 M in CH_2Cl_2 at 100 $mV\cdot s^{-1}$) of the ligand **L** and complexes **1** and **2**.

	$E^1_{1/2}$/V		$E^2_{1/2}$/V		$E^3_{1/2}$/V	
	$^{Ox}E^1_{1/2}$	$^{red}E^1_{1/2}$	$^{Ox}E^2_{1/2}$	$^{red}E^2_{1/2}$	$^{Ox}E^3_{1/2}$	$^{red}E^3_{1/2}$
L	0.79	0.70	1.17	1.09	/	/
1	0.76	0.67	1.15	1.02	1.28	1.20
2	0.76	0.66	1.13	0.99	1.28	1.20

The cyclic voltammogram for **L** shows two mono-electronic oxidations at about 0.75 and 1.13 V, corresponding to the formation of a radical cation and a dication TTF fragment, respectively (Figure S1). These oxidation potentials are higher than those found for the functionalized TTF donor used in the synthesis of the other dinuclear complexes, due to the direct functionalization of the TTF core with two methyl ester groups [57,58]. The electrochemistry does not highlight significant effects on the oxidation potentials upon coordination of the electron attracting $Ln(hfac)_3$ fragments (Table 3). Nevertheless, an additional quasi-reversible oxidation wave is observed for the two complexes around 1.24 V. No clear

explanation can be given for the origin of this additional redox activity at this point. The reversibility of the oxidation potentials is conserved and the electrochemical properties attest to the redox activity of **L** in the complexes.

2.4. Photo-Physical Properties

2.4.1. Absorption Properties

The UV-visible absorption properties of **L** and **2** have been studied in a CH_2Cl_2 solution and in a KBr pellet in solid-state (Figures 3a and 4a, Figures S2 and S3). Rationalization by TD-DFT calculations was performed on **L** and the Y(III) analogue of **1** and **2** (Figures 3b and 4b) following a computational strategy already used successfully on TTF-based systems [62]. The molecular orbital diagram is sketched in Figure 5.

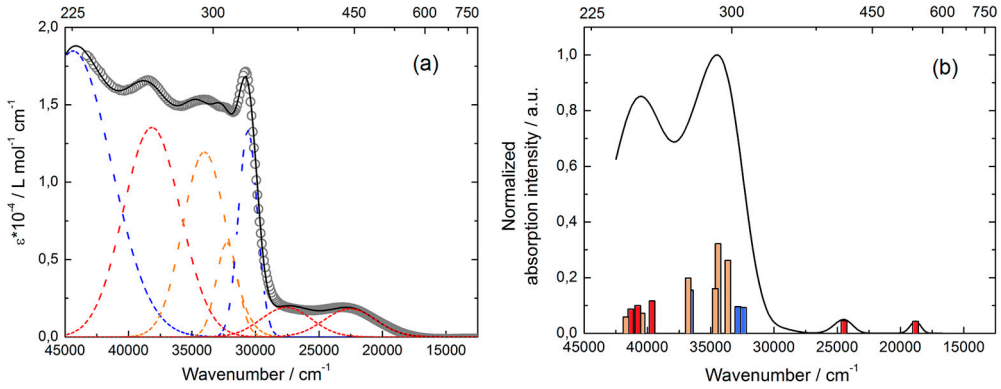

Figure 3. (**a**) Experimental UV-visible absorption spectra of **L** in CH_2Cl_2 solution (C = 4×10^{-5} mol·L^{-1}) (open grey circles). Respective Gaussian decompositions (red, orange, and blue dashed lines correspond to ILCT, intra-donor and intra-acceptor transitions, respectively) and best fit (full black line) (R = 0.9994) (**b**) Theoretical absorption spectra of **L** (black line). The bars represent the mean contributions of the absorption spectra.

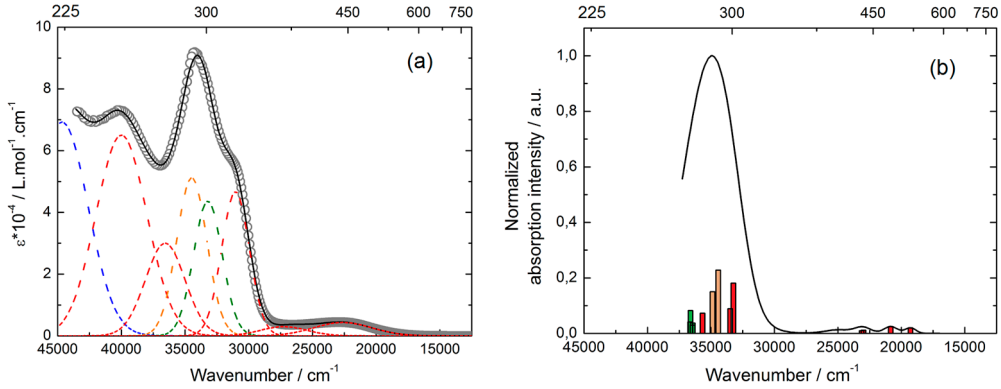

Figure 4. (**a**) Experimental UV-visible absorption spectra in CH_2Cl_2 solution of **2** (C = 4×10^{-5} mol·L^{-1}) (open grey circles). Respective Gaussian decompositions (green dashed line corresponds to intra-hfac transitions) and best fit (full black line) (R = 0.9998); (**b**) Theoretical absorption spectra of the Y^{III} analogue (black line). The bars represent the mean contributions of the absorption spectra.

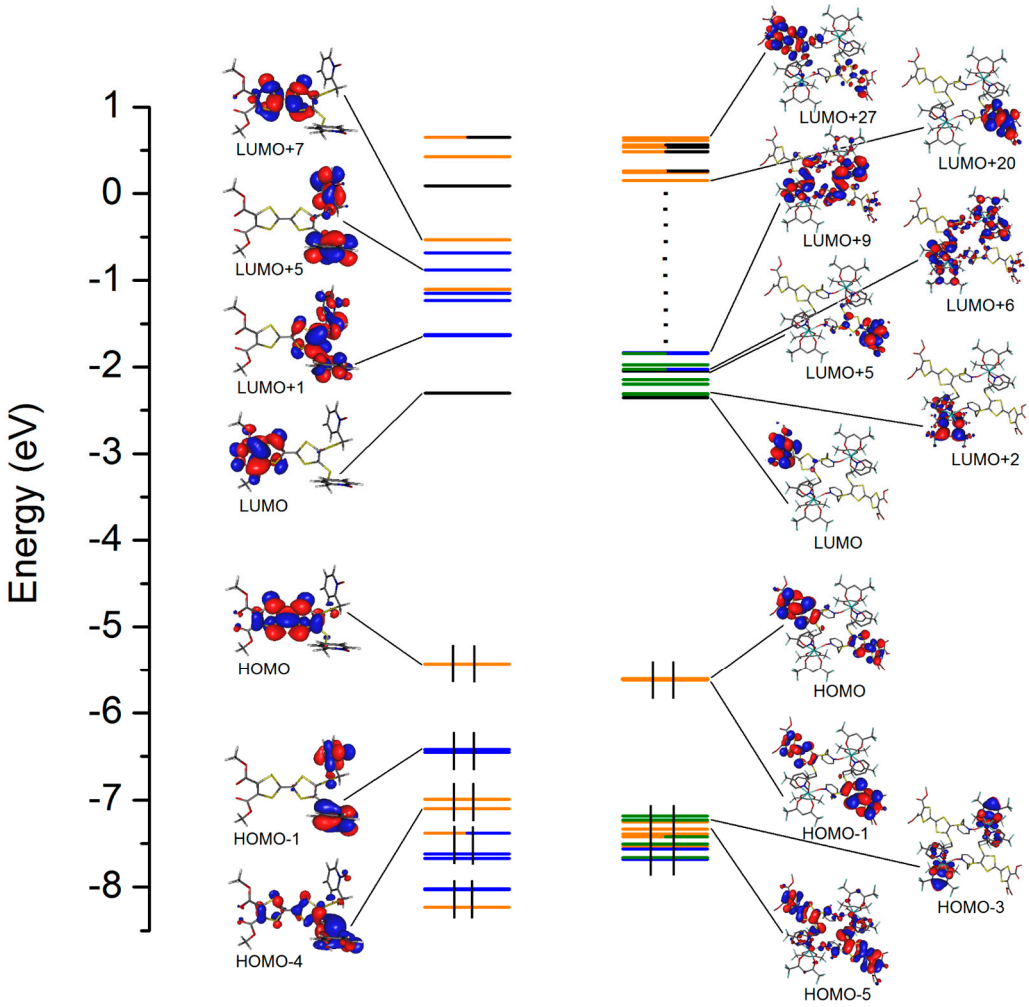

Figure 5. Molecular orbital diagram for **L** (**left**) and the Y^{III} analogue (**right**). The energy levels of the centred TTF, 2-methylpyridine-*N*-oxide, methyl ester, and $hfac^-$ orbitals are represented in orange, blue, black, and green, respectively.

The experimental absorption curve of **L** has been decomposed into seven bands (Figures 3a and S2, Table 4). The calculated UV-visible absorption spectrum for **L** reproduces the experimental curve well (Figure 3b). The low energy bands (red Gaussian decomposition) were attributed to π–π* HOMO→LUMO and HOMO→LUMO + 1 excitations. While the latter is identified as the classical TTF to Methyl-2-Py-*N*-oxide charge transfer (ILCT) (Table 4) [57,58], the lowest-energy excitation is identified as TTF to methyl ester charge transfer. Thus, the functionalization of the TTF core with methyl ester groups has successfully increased the intensity of the ILCT and induced the appearance of new ILCT at lower-energy (22,600 cm^{-1}, calculated at 18,810 cm^{-1}) than the TTF to Methyl-2-Py-*N*-oxide ILCT (27,600 cm^{-1}, calculated at 24,463 cm^{-1}). The remaining absorption bands were respectively identified as Intra-Acceptor (IA) (where the acceptor is the Py-*N*-oxide moiety), Intra-donor (ID), and ILCT excitations (Table 4).

Table 4. TD-DFT calculated excitations energies and main composition of low-lying electronic transitions for **L** and the **Y**(III) analogue of **1** and **2**. In addition, charge transfer and the pure intramolecular transitions are reported. ID, IA, Ihfac, H, and L represent respectively the intramolecular TTF (Donor), 2-pyridine-*N*-oxide (Py) (Acceptor) or $hfac^-$ ligand, HOMO and LUMO; therefore ILCT stands for Intra-Ligand Charge Transfer (from TTF to 2-pyridine-*N*-oxide (PyNO) or methyl ester (ester)). The theoretical values are evaluated at the PCM(CH_2Cl_2)-PBE0/SVP level of approximation. Bold style is used to highlight the main contributions. Exp.: experimental, Th.: theoretical, Osc.: oscillator strength.

	Energy Exp. (cm^{-1})	Energy Th. (cm^{-1})	Osc.	Type	Assignment	Transition
L	22,600	18,810	0.03	ILCT	$\pi_{TTF}\rightarrow\pi^*_{Ester}$	H→L (99%)
	27,600	24,463	0.03	ILCT	$\pi_{TTF}\rightarrow\pi^*_{PyNO}$	H→L + 1 (88%)
	30,600	32,414	0.06	IA	$\pi_{PyNO}\rightarrow\pi^*_{PyNO}$	H-1→L + 1 (74%)
		32,857	0.07			H-2→L + 1 (70%)
	32,200	33,652	0.18	**ID** + ILCT	$\boldsymbol{\pi_{TTF}\rightarrow\pi^*_{TTF}}$ + $\pi_{TTF}\rightarrow\pi^*_{PyNO}$	**H→L + 7 (60%)**
		34,426	0.22			H-3/-4→L + 1 (43/28%)
		34,640	0.11			
	34,000	36,605	0.11	**ID** + IA	$\boldsymbol{\pi_{TTF}\rightarrow\pi^*_{TTF}}$ + $\pi_{PyNO}\rightarrow\pi^*_{PyNO}$	**H→L + 7/ + 9 (10/44%)**
		36,788	0.14			H-1→L + 2/ + 5/ + 6 (9/27/10%)
	38,200	39,635	0.08	ID + **ILCT**	$\pi_{TTF}\rightarrow\pi^*_{TTF}$ + $\boldsymbol{\pi_{TTF}\rightarrow\pi^*_{PyNO}}$	H-3/-4→L + 4 (38/40%)
		40,437	0.05			**H-5→L + 1 (38%)**
		40,773	0.07			**H-3→L + 2 (25%)**
		41,331	0.06			**H-10→L (41%)**
		41,698	0.04			
	44,400	/	/	IA	$\pi_{PyNO}\rightarrow\pi^*_{PyNO}$	/
Y	22,600	19,282	0.03	ILCT	$\pi_{TTF}\rightarrow\pi^*_{Ester}$	H/-1→L (76/22%)
		20,840	0.04			H/-1→L + 5 (22/72%)
	27,300	22,985	0.02	ILCT	$\pi_{TTF}\rightarrow\pi^*_{PyNO}$	H→L + 6/ + 8/ + 9 (20/19/21%)
		23,132	0.02			H-1→L + 6/ + 9 (17/33%)
	31,000	33,234	0.30	ID + **ILCT**	$\pi_{TTF}\rightarrow\pi^*_{TTF}$ + $\boldsymbol{\pi_{TTF}\rightarrow\pi^*_{Ester}}$	H/-1→L + 20 (9/30%)
		33,485	0.15			H→L + 21 (15%)
						H-4/-5→L (21/29%)
	33,200	36,440	0.27	Ihfac	$\pi_{hfac}\rightarrow\pi^*_{hfac}$	H→L + 10 (53%)
		36,455				+
		36,618	0.10			H-3→L (65%)
		36,639				
	34,500	34,432	0.38	ID	$\pi_{TTF}\rightarrow\pi^*_{TTF}$	H/-1→L + 21 (12/41%)
		34,886				H/-1→L + 22 (9/30%)
	36,600	35,662	0.12	ILCT	$\pi_{TTF}\rightarrow\pi^*_{Ester}$	H-4/-5→L + 5 (13/7%)
	40,000	/	/	ILCT	$\pi_{TTF}\rightarrow\pi^*_{PyNO}$	/
	44,700	/	/	IA	$\pi_{L2}\rightarrow\pi^*_{PyImPy}$	/

For **2**, the absorption spectrum has been decomposed into eight bands for the solution and solid-state measurements.

The absorption spectra for the free ligand and the dinuclear complex are similar. Only an additional intense absorption band is observed around 33,000 cm^{-1} that corresponds to π–π* intra-$hfac^-$ excitations [62]. Complexation induces a very weak red shift of the ILCT transitions involving the Py-*N*-oxide acceptor (300 cm^{-1}, calculated red shift 1400 cm^{-1}), due to the Lewis acid behaviour of the $Ln(hfac)_3$ moieties enforcing the electron withdrawing character of the 2-pyridine-*N*-oxide fragments. This effect is weak because of the poor electronic communication through the methylthio arms. Nevertheless, the red-shift of these absorption bands in coordination complexes compared to those in **L** is a first indication of the stability of the dinuclear complexes in such solvents.

2.4.2. Emission Properties

No significant emission for the free ligand was detected, as already observed in previous TTF-based ligands in which the TTF core is not conjugated with the coordinated moieties [57,58]. Emission properties of **2** were measured in solid state at 77 K (Figure 6). The characteristic luminescence profile of Yb^{III}, corresponding to the $^2F_{5/2} \rightarrow {}^2F_{7/2}$ transition, is observed upon irradiation at 22,222 cm^{-1} (450 nm). This low-energy irradiation is possible due to the ILCT involving the methyl ester groups. No residual emission centred on the ligand **L** was observed in the visible range after coordination. Based on the previous published TTF-based complexes of Yb^{III} [57,63,64], it is expected that in the antenna-effect sensitization process, such energy transfer takes place between the singlet CT excited state of the chromophore to the $^2F_{5/2}$ states of the Yb^{III} ion.

Four main emission maxima are clearly identified at the following energies: 9718, 9843, 9980, and 10,204 cm^{-1}. The total splitting is determined to be equal to 486 cm^{-1}. The values of this splitting for an Yb^{III} ion in a distorted and regular D_3 symmetry are 455 and 372 cm^{-1}, respectively [65], while a splitting of 528 cm^{-1} is found for an Yb complex in a lower symmetry, increasing up to 880 cm^{-1} for organometallic derivatives [66]. The value of 486 cm^{-1} thus seems to correspond to a quite low symmetry. Nevertheless, this value is lower than the one found in a dinuclear analogue (508 cm^{-1}) in which the distortion of the square anti-prism symmetry of the Yb^{III} coordination sphere is more pronounced ($CShM_{SAPR-8}$ = 0.484).

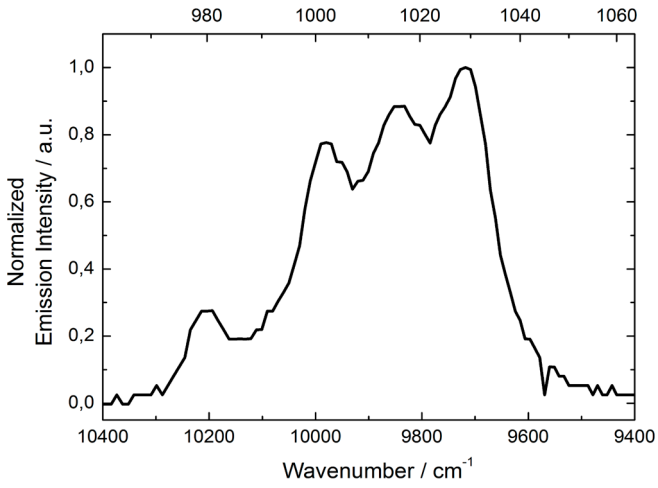

Figure 6. Luminescence spectrum of **2** in the Near Infrared (NIR) range for λ_{ex} = 22,222 cm^{-1} (450 nm) in solid-state at 77 K.

2.5. Magnetic Properties

The temperature dependence of $\chi_M T$, with χ_M being the molar magnetic susceptibility and T being the temperature in Kelvin, in powdered samples of compounds **1** and **2** are represented in Figure 7. The room temperature values are equal to 27.6 and 4.69 $cm^3\ K{\cdot}mol^{-1}$ for **1** and **2**, respectively. These values are in good agreement with the two expected values for the two multiplet ground states: $^6H_{15/2}$ (14.17 × 2 $cm^3\ K{\cdot}mol^{-1}$) and $^2F_{7/2}$ (2.57 × 2 $cm^3\ K{\cdot}mol^{-1}$) for two Dy^{III} and two Yb^{III} ions, respectively [67]. $\chi_M T$ decreases on cooling due to the crystal field splitting of the multiplet ground states down to 20.2 $cm^3{\cdot}K{\cdot}mol^{-1}$ for **1**, and 1.03 $cm^3{\cdot}K{\cdot}mol^{-1}$ for **2**. At 2 K, the magnetization saturates around 10 Nβ for **1** and 2.8 Nβ for **2**. Neither of the two complexes show frequency dependence of ac susceptibility.

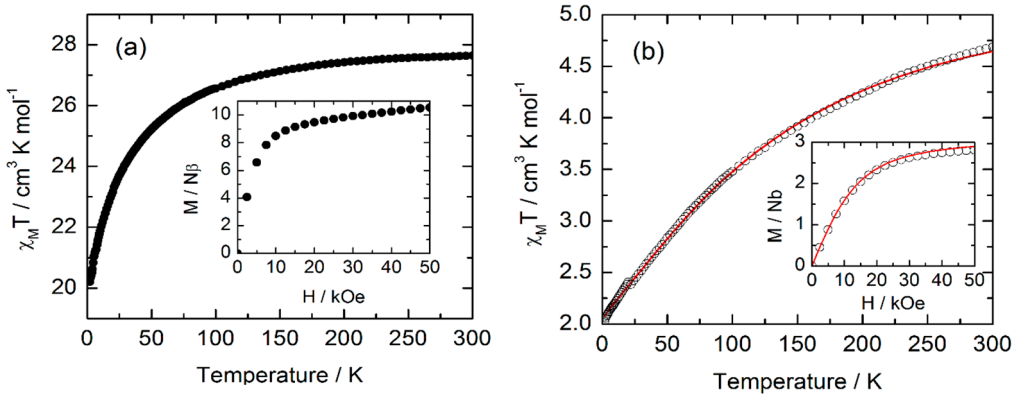

Figure 7. (**a**) Temperature dependence of $\chi_M T$ for **1**. Inset: field variation of the magnetization measured at 2 K; (**b**) Temperature dependence of $\chi_M T$ for **2**. Inset: field variation of the magnetization measured at 2 K. The red line corresponds to the best-fitted curve (see text). χ_M, molar magnetic susceptibility; T, temperature in Kelvin.

2.6. Correlation Magnetism-Luminescence

In the last five years, we have proven that magnetism and luminescence are intimately correlated [50,54,56,57,64]. In the case of compound **2**, the excitation $^2F_{5/2} \rightarrow {}^2F_{7/2}$ can be viewed as a picture of the crystal field splitting of the ground state multiplet, while temperature dependence of the magnetic response can be viewed as a thermal picture of the same ground state multiplet splitting. In the first approximation, the coordination polyhedron of Yb^{III} in **2** has a D_{4d} symmetry ($CShM_{SAPR\text{-}8}$~0.4), with an environment close to an antiprismatic square. In this approximation, and in the formalism of Stevens, the ground state splitting can be accounted for by the following Hamiltonian for one metallic centre:

$$\hat{H} = B_2^0\widehat{O_2^0} + B_4^0\widehat{O_4^0} + B_6^0\widehat{O_6^0}$$

Where $\widehat{O_k^q}$ are the operators equivalents expressed as polynomials of the total angular momentum ($\hat{J^2}$, $\hat{J_z}$, $\hat{J_+}$, and $\hat{J_-}$), and B_k^q are connected to the crystal field parameters [68,69]. The perturbation due to the application of an external magnetic field can be easily estimated and the magnetization calculated. In a D_{4d} environment, only the terms with q = 0 and k = 2, 4, and 6 are non zero [70]. The temperature variation of $\chi_M T$ in **2** is fitted and the best curve is represented in Figure 7b (Yb1 and Yb2 are treated identically since they have a very similar environment). To ensure that the obtained set of parameters is correct, the M *vs.* H curve is also calculated at 2 K (inset of Figure 7b). In a D_{4d} symmetry M_J is a good

quantum number, so the eigenstates are pure M_J states. In this frame, the ground state corresponds to $M_J = \pm 5/2$, which is taken at the energy origin. The first excited state ($M_J = \pm 3/2$) is located at 215 cm^{-1}, the second at 468 cm^{-1}, and the last at 569 cm^{-1} above the ground state. The gap between the first two levels almost perfectly matches the gap between the two emission lines at 10,204 and 9980 cm^{-1}. The last two emission lines (9843 and 9780 cm^{-1}) are not so well reproduced, which might be due to the relative insensitivity of the magnetism to the high energy levels. Indeed, the last two levels are almost not thermally populated, even at room temperature.

3. Experimental Section

3.1. Synthesis

General Procedures and Materials: The precursors $Ln(hfac)_3 \cdot 2H_2O$ (Ln = Dy^{III} and Yb^{III}, $hfac^-$ = 1,1,1,5,5,5-hexafluoroacetylacetonate anion) [71] and the 4,5-dicarboxylic acid-4′,5′-bis(2-cyanoethyl)thio)-tetrathiafulvalene-, dimethyl ester [59] were synthesised following previously reported methods. All other reagents were purchased from Aldrich Co., Ltd. (Saint-Quentin Fallavier, France) and used without further purification.

*3.2. Synthesis of 4,5-Bis(2-Pyridyl-N-Oxidemethylthio)-4',5'-Dicarboxylic Acid-Tetrathiafulvalene-, Dimethyl Ester (**L**)*

Method A. A solution of 0.5 M EtONa/EtOH (14 mL) was added to a suspension of 4,5-dicarboxylic acid-4′,5′-bis(2-cyanoethyl)thio)-tetrathiafulvalene-, dimethyl ester [72] (0.676 g, 1.38 mmol) in anhydrous degassed EtOH (41 mL) under argon. After being stirred at room temperature for 4 h, the mixture was reacted with a solution of 2-(chloromethyl)pyridine-1-oxide [73] (0.593 g, 4.13 mmol) in anhydrous degassed EtOH (27 mL), and then the mixture was stirred for 16 h. H_2O (41 mL) was added to quench the reaction, and the mixture was poured into CH_2Cl_2 (345 mL), washed with saturated $NaHCO_3$ (3 × 55 mL) and water (210 mL). The organic extract was concentrated in vacuum to give a red-brown oil, which was purified by chromatography on alumina gel, initially with CH_2Cl_2 (to remove the unreacted alkyl halide), and then with CH_2Cl_2/MeOH (10:1) to give the pure desired ligand. Yield: 437 mg (53%). Anal. Calcd (%) for $C_{22}H_{18}N_2O_6S_6$: C 44.15, H 3.01, N 4.68; found: C 44.03, H 3.05, N 4.74. ^{1}H-NMR ($CDCl_3$): 8.24–8.20 (m, 4H), 7.31–7.17 (m, 4H), 3.80 (s, 6H), 3.34 (s, 4H). I.R. (KBr): 2967 (w), 1738 (s), 1724 (s), 1584 (m), 1428 (m), 1415 (m), 1253 (s), 1092 (m), 1020 (m), 886 (w), and 769 (w) cm^{-1}.

Method B. $CsOH \cdot H_2O$ (335 mg, 2.00 mmol) dissolved in a minimum of MeOH was slowly added to 4,5-dicarboxylic acid-4′,5′-bis(2-cyanoethyl)thio)-tetrathiafulvalene-, dimethyl ester (0.490 g, 1.00 mmol) in 10 mL of DMF. After being stirred at room temperature for 30 min, the mixture was reacted with a solution of 2-(chloromethyl)pyridine-1-oxide [73] (0.430 g, 2.99 mmol) in anhydrous degassed MeOH (25 mL), and then the mixture was stirred overnight. Then the organic solvents were removed under vacuum and the residue extracted with CH_2Cl_2 and washed with H_2O. The organic phase was extracted and dried with $MgSO_4$. Pure ligand was obtained by chromatography on alumina gel, initially with CH_2Cl_2 (to remove the unreacted alkyl halide) and then with CH_2Cl_2/MeOH (10:1). Yield: 486 mg (59%).

*3.3. Synthesis of Complexes **1** and **2***

$[Dy_2(hfac)_6(L)_2]\cdot CH_2Cl_2\cdot(C_6H_{14})_{0.5}$ (**1**). 32.8 mg of $Dy(hfac)_3\cdot 2H_2O$ (0.04 mmol) were dissolved in 10 mL of CH_2Cl_2 and then added to a solution of 10 mL of CH_2Cl_2 containing 24.0 mg of **L** (0.04 mmol). After 15 min of stirring, 25 mL of *n*-hexane were layered at room temperature in the dark. Slow diffusion leads to dark red single crystals, which are suitable for X-ray studies. Yield: 100 mg (86%). Anal. Calcd (%) for $C_{75}H_{44}Cl_2Dy_2F_{36}N_4O_{24}S_{12}$: C 31.58, H 1.54, N 1.97; found: C 31.69, H 1.62 N, 2.01. I.R. (KBr): 2956 (w), 2928 (w), 2870 (w), 1734 (m), 1653 (s), 1556 (m), 1531 (m), 1508 (m), 1447 (w), 1256 (s), 1211 (s), 1144 (s), 1101 (w), 798 (w), 769 (w), 661 (m), and 587 (w) cm^{-1}.

$[Yb_2(hfac)_6(L)_2]\cdot CH_2Cl_2\cdot(C_6H_{14})_{0.5}$ (**2**). This compound was obtained using the same protocol as for **1**, starting from 33.2 mg of $Yb(hfac)_3\cdot 2H_2O$ (0.04 mmol) instead of $Dy(hfac)_3\cdot 2H_2O$. Yield: 82 mg (71%). Anal. Calcd (%) for $C_{75}H_{44}Cl_2Yb_2F_{36}N_4O_{24}S_{12}$: C 31.47, H 1.54, N 1.96; found: C 31.57, H 1.60, N, 2.03. I.R. (KBr): 2954 (w), 2928 (w), 2871 (w), 1734 (m), 1657 (s), 1558 (m), 1533 (m), 1513 (m), 1448 (w), 1264 (s), 1216 (s), 1151 (s), 799 (w), 769 (w), 662 (m), and 588 (w) cm^{-1}.

3.4. Crystallography

A single crystal of **1** was mounted on a APEXII Bruker-AXS diffractometer for data collection (MoK_α radiation source, $\lambda = 0.71073$ Å), at the Centre de Diffractométrie (CDIFX), Université de Rennes 1, France. The structure was solved with a direct method using the SIR-97 program and refined with a full matrix least-squares method on F^2 using the SHELXL-97 program [74,75]. Crystallographic data are summarized in Table 1. Complete crystal structure results as a CIF file including bond lengths, angles, and atomic coordinates are deposited as Supplementary files.

3.5. Physical Measurements

The elementary analyses of the compounds were performed at the Centre Régional de Mesures Physiques de l'Ouest, Rennes. Cyclic voltammetry was carried out in CH_2Cl_2 solution, containing 0.1 M $N(C_4H_9)_4PF_6$ as supporting electrolyte. Voltammograms were recorded at 100 $mV\cdot s^{-1}$ with a platinum disk electrode. The potentials were measured *versus* a saturated calomel electrode (SCE). Absorption spectra were recorded on a Varian Cary 5000 UV-Visible-NIR spectrometer equipped with an integration sphere. The luminescence spectra were measured using a Horiba-Jobin Yvon Fluorolog-3® spectrofluorimeter, equipped with a three slit double grating excitation and emission monochromator with dispersions of 2.1 nm/mm (1200 grooves/mm). The steady-state luminescence was excited by unpolarized light from a 450 W xenon CW lamp. Quartz tubes containing the samples were immersed in liquid nitrogen and near infra-red spectra were recorded at right angle using a liquid nitrogen cooled, solid indium/gallium/arsenic detector (850–1600 nm). Spectra were reference corrected for both the excitation source light intensity variation (lamp and grating) and the emission spectral response (detector and grating). The dc magnetic susceptibility measurements were performed on a solid polycrystalline sample with a Quantum Design MPMS-XL SQUID magnetometer between 2 and 300 K in applied magnetic field of 0.2 T for temperatures of 2–20 K and 1 T for temperatures of 20–300 K. These measurements were all corrected for the diamagnetic contribution calculated with Pascal's constants.

3.6. Computational Details

DFT geometry optimizations and TD-DFT excitation energy calculations of the ligand **L** and Y^{III} analogue of the dinuclear complexes were carried out with the Gaussian 09 (revision A.02) package [76] employing the PBE0 hybrid functional [77,78]. The "Stuttgart/Dresden" basis sets and effective core potentials were used to describe the yttrium atom [79], whereas all other atoms were described with the SVP basis sets [80]. The first 50 monoelectronic excitations were calculated for ligand **L** while the first 100 monoelectronic excitations were calculated for the Y^{III} analogue of the dinuclear complexes. In all steps, a modelling of bulk solvent effects (solvent = dichloromethane) was included through the Polarisable Continuum Model (PCM) [81], using a linear-response non-equilibrium approach for the TD-DFT step [82,83]. Molecular orbitals were sketched using the Gabedit graphical interface [84].

4. Conclusions

Two dinuclear complexes of formula $[Ln_2(hfac)_6(\mathbf{L})_2]\cdot CH_2Cl_2\cdot(C_6H_{14})_{0.5}$ (Ln = Dy (**1**) and Yb (**2**)) have been synthesised. The analysis of the polyhedron symmetry around the metallic centres reveals that the dinuclear complexes of the present work have the most symmetric coordination sphere (square anti-prism symmetry) compared to the previously published dinuclear compounds. Nevertheless, they do not display any out-of phase signals of their magnetic susceptibility, demonstrating that the symmetry of the coordination polyhedron is not the crucial parameter for displaying slow magnetic relaxation, but it might be the electronic distribution of the first neighbouring atoms. The functionalization of the TTF core with two methyl ester groups leads to a low-energy ILCT band, which is identified as the HOMO→LUMO excitation. The LUMO is localized on the methyl ester moieties. Irradiation of this absorption band leads to the sensitization of the Yb^{III}-centred luminescence. Static magnetic properties of the Yb^{III} analogue and its luminescence have been correlated. More work is in progress in the group in order to assemble this kind of dinuclear complexes through chemical modifications of the methyl ester groups, for example using carboxylic functions.

Supplementary Materials

Supplementary materials can be found at http://www.mdpi.com/2304-6740/3/4/0554/s1.

Acknowledgments

This work was supported by the CNRS, Rennes Métropole, Université de Rennes 1, Région Bretagne, FEDER and Agence Nationale de la Recherche (No. ANR-13-BS07-0022-01). Boris Le Guennic thanks the French GENCI-CINES center for high-performance computing resources (project x2015080649).

Author Contributions

Fabrice Pointillart, Saskia Speed and Bertrand Lefeuvre performed the syntheses and characterizations. Stéphane Golhen and Lahcène Ouahab performed single crystal X-ray diffraction analyses. François Riobé and Olivier Maury did the luminescence measurements and analyses. Boris Le Guennic performed the calculations and Olivier Cador the magnetic measurements.

Conflicts of Interest

The authors declare no conflict of interest.

References

1. Ishikawa, N.; Sugita, M.; Ishikawa, T.; Koshihara, S.; Kaizu, Y. Lanthanide double-decker complexes functioning as magnets at the single-molecular level. *J. Am. Chem. Soc.* **2003**, *125*, 8694–8695.
2. Woodruff, D.N.; Winpenny, R.E.P.; Layfield, R.A. Lanthanide single-molecule magnets. *Chem. Rev.* **2013**, *113*, 5110–5148.
3. Luzon, J.; Sessoli, R. Lanthanides in molecular magnetism: So fascinating so challenging. *Dalton Trans.* **2012**, *41*, 13556–13567.
4. Sessoli, R.; Powell, A.K. Strategies towards single molecule magnets based on lanthanide ions. *Coord. Chem. Rev.* **2009**, *253*, 2328–2341.
5. Layfield, R.A. Organometallic single-molecule magnets. *Organometallics* **2014**, *33*, 1084–1099.
6. Feltham, H.L.C.; Brooker, S. Review of purely 4f and mixed-metal nd-4f single-molecule magnets containing only lanthanide ion. *Coord. Chem. Rev.* **2014**, *276*, 1–33.
7. Benelli, C.; Gatteschi, D. Magnetism of lanthanides in molecular materials with transition-metal ions and organic radicals. *Chem. Rev.* **2002**, *102*, 2369–2387.
8. Zhang, P.; Guo, Y.-N.; Tang, J. Recent advances in dysprosium-based single molecule magnets: Structural overview and synthetic strategies. *Coord. Chem. Rev.* **2013**, *257*, 1728–1763.
9. Zhang, P.; Zhang, L.; Tang, J. Lanthanide single molecule magnets: Progress and perspective. *Dalton Trans.* **2015**, *44*, 3923–3929.
10. Ungur, L.; Lin, S.-Y.; Tang, J.; Chibotaru, L.F. Single-molecule toroics in Ising-type lanthanide molecular clusters. *Chem. Soc. Rev.* **2014**, *43*, 6894–6905.
11. Liddle, S.T.; van Slageren, J. Improving f-element single molecule magnets. *Chem. Soc. Rev.* **2015**, *44*, 6655–6669.
12. Bünzli, J.C.G.; Piguet, C. Lanthanide-containing molecular and supramolecular polymetallic functional assemblies. *Chem. Rev.* **2002**, *102*, 1897–1928.
13. Moro, F.; Mills, D.P.; Liddle, S.T.; van Slageren, J. The inherent single-molecule magnet character of trivalent uranium. *Angew. Chem. Int. Ed.* **2013**, *52*, 3430–3433.
14. Coutinho, J.T.; Antunes, M.A.; Pereira, L.C.J.; Marçalo, J.; Almeida, M. Zero-field slow magnetic relaxation in a uranium(III) complex with a radical ligand. *Chem. Commun.* **2014**, *50*, 10262–10264.
15. King, D.M.; Tuna, F.; McMaster, J.; Lewis, W.; Blake, A.J.; McInnes, E.J.L.; Liddle, S.T. Single-molecule magnetism in a single-ion triamidoamine uranium(V) terminal mono-oxo complex. *Angew. Chem. Int. Ed.* **2013**, *52*, 4921–4924.
16. Mougel, V.; Chatelain, L.; Pécaut, J.; Caciuffo, R.; Colineau, E.; Griveau, J.-C.; Mazzanti, M. Uranium and manganese assembled in a wheel-shaped nanoscale single-molecule magnet with high spin-reversal barrier. *Nat. Chem.* **2012**, *4*, 1011–1017.
17. Magnani, N.; Colineau, E.; Griveau, J.-C.; Apostolidis, C.; Walter, O.; Caciuffo, R. A plutonium-based single-molecule magnet. *Chem. Commun.* **2014**, *50*, 8171–8173.

18. Meihaus, K.R.; Minasian, S.G.; Lukens, W.W., Jr.; Kozimor, S.A.; Shuh, D.K.; Tyliszczak, T.; Long, J.R. Influence of pyrazolate *vs*. *N*-heterocyclic carbene ligands on the slow magnetic relaxation of homoleptic trischelate lanthanide(III) and uranium(III) complexes. *J. Am. Chem. Soc.* **2014**, *136*, 6056–6068.
19. Le Roy, J.J.; Gorelsky, S.I.; Korobkov, I.; Murugesu, M. Slow magnetic relaxation in uranium(III) and neodymium(III) cyclooctatetraenyl complexes. *Organometallics* **2015**, *34*, 1415–1418.
20. Dei, A.; Gatteschi, D. Molecular (Nano) magnet as test grounds of quantum mechanics. *Angew. Chem. Int. Ed.* **2011**, *50*, 11852–11858.
21. Leuenberger, M.N.; Loss, D. Quantum computing in molecular magnets. *Nature* **2001**, *410*, 789–793.
22. Hill, S.; Edwards, R.S.; Aliaga-Alcalde, N.; Christou, G. Quantum coherence in an exchange-coupled dimer of single-molecule magnets. *Science* **2003**, *302*, 1015–1018.
23. Hosseini, M.W.; Rebic, S.; Sparkes, B.M.; Twamley, J.; Buchler, B.C.; Lam, P.K. Memory-enhanced noiseless cross-phase modulation. *Light Sci. Appl.* **2012**, *1*, e40, doi:10.1038/lsa.2012.40.
24. Sessoli, R.; Tsai, H.L.; Schake, A.R.; Wang, S.; Vincent, J.B.; Folting, K.; Gatteschi, D.; Christou, G.; Hendrickson, D.N. High-spin molecules: $[Mn_{12}O_{12}(O_2CR)_{16}(H_2O)_4]$. *J. Am. Chem. Soc.* **1993**, *115*, 1804–1816.
25. Mannini, M.; Pineider, F.; Sainctavit, P.; Danieli, C.; Otero, E.; Sciancalepore, C.; Talarico, A.M.; Arrio, M.-A.; Cornia, A.; Gatteschi, D.; *et al*. Magnetic memory of a single-molecule quantum magnet wired to a gold surface. *Nat. Mater.* **2009**, *8*, 194–197.
26. Gu, M.; Li, X.; Cao, Y. Optical storage arrays: A perspective for future big data storage. *Light Sci. Appl.* **2014**, *3*, e177, doi:10.1038/lsa.2014.58.
27. Papasimakis, N.; Thongrattanasiri, S.; Zheludev, N.I.; de Abajo, F.J. The magnetic response of grapheme split-ring metamaterials. *Light Sci. Appl.* **2013**, *2*, e78, doi:10.1038/lsa.2013.34.
28. Sanvito, S. Molecular Spintronics. *Chem. Soc. Rev.* **2011**, *40*, 3336–3355.
29. Bogani, L.; Wernsdorfer, W. Molecular spintronics using single-molecule magnets. *Nat. Mater.* **2008**, *7*, 179–186.
30. De Bettancourt-Dias, A. *Luminescence of Lanthanide Ions in Coordination Compounds and Nanomaterials*; Wiley: Hoboken, NJ, USA, 2014.
31. Weissman, S.I. Intramolecular energy transfer, the fluorescence of complexes of europium. *J. Chem. Phys.* **1942**, *10*, 214–217.
32. Crosby, G.A.; Kasha, M. Intramolecular energy transfer in ytterbium organic chelates. *Spectrochim. Acta* **1958**, *10*, 377–382.
33. Lin, S.-Y.; Wang, C.; Zhao, L.; Wua, J.; Tang, J. Chiral mononuclear lanthanide complexes and field-induced single-ion magnet behaviour of Dy analogue. *Dalton Trans.* **2015**, *44*, 223–229.
34. Long, J.; Rouquette, J.; Thibaud, J.-M.; Ferreira, R.A.S.; Carlos, L.D.; Donnadieu, B.; Vieru, V.; Chibotaru, L.F.; Konczewicz, L.; Haines, J.; *et al*. A high-temperature molecular ferroelectric Zn/Dy complex exhibiting single-ion-magnet behavior and lanthanide luminescence. *Angew. Chem. Int. Ed.* **2015**, *54*, 2236–2240.
35. Li, X.-L.; Chen, C.-L.; Xiao, H.-P.; Wang, A.-L.; Liu, C.-M.; Zheng, X.; Gao, L.-J.; Yanga, X.-G.; Fang, S.-M. Luminescent, magnetic and ferroelectric properties of noncentrosymmetric chain-like complexes composed of nine-coordinate lanthanide ions. *Dalton Trans.* **2013**, *42*, 15317–15325.

36. Tanaka, H.; Kobayashi, H.; Kobayashi, A.; Cassoux, P. Superconductivity, antiferromagnetism, and phase diagram of a series of organic conductors: λ-$(BETS)_2Fe_xGa_{1-x}Br_yCl_{4-y}$. *Adv. Mater.* **2000**, *12*, 1685–1689.
37. Uji, S.; Shinagawa, H.; Terashima, T.; Terakura, C.; Yakabe, T.; Terai, Y.; Tokumoto, M.; Kobayashi, A.; Tanaka, H.; Kobayashi, H. Magnetic-field-induced superconductivity in a two-dimensional organic conductor. *Nature* **2001**, *410*, 908–910.
38. Kobayashi, A.; Fujiwara, E.; Kobayashi, H. Single-component molecular metals with extended-TTF dithiolate ligands. *Chem. Rev.* **2004**, *104*, 5243–5264.
39. Enoki, T.; Miyasaki, A. Magnetic TTF-based charge-transfer complexes. *Chem. Rev.* **2004**, *104*, 5449–5478.
40. Coronado, E.; Day, P. Magnetic molecular conductors. *Chem. Rev.* **2004**, *104*, 5419–5448.
41. Ouahab, L.; Enoki, T. Multiproperty molecular materials: TTF-based conductiong and magnetic molecular materials. *Eur. J. Inorg. Chem.* **2004**, *2004*, 933–941.
42. Fujiwara, H.; Wada, K.; Hiraoka, T.; Hayashi, T.; Sugimoto, T.; Nakazumi, H.; Yokogawa, K.; Teramura, M.; Yasuzuka, S.; Murata, K.; *et al*. Stable metallic behavior and antiferromagnetic ordering of Fe(III) *d* spins in $(EDO\text{-}TTFVO)_2 \cdot FeCl_4$. *J. Am. Chem. Soc.* **2005**, *127*, 14166–14167.
43. Lorcy, D.; Bellec, N.; Fourmigué, M.; Avarvari, N. Tetrathiafulvalene-based group XV ligands: Synthesis, coordination chemistry and radical cation salts. *Coord. Chem. Rev.* **2009**, *253*, 1398–1438.
44. Pointillart, F.; Golhen, S.; Cador, O.; Ouahab, L. Paramagnetic 3D coordination complexes involving redox-active tetrathiafulvalene derivatives: An efficient approach to elaborate multi-properties materials. *Dalton Trans.* **2013**, *42*, 1949–1960.
45. Cosquer, G.; Pointillart, F.; Golhen, S.; Cador, O.; Ouahab, L. Slow magnetic relaxation in condensed *versus* dispersed dysprosium(III) mononuclear complexes. *Chem. Eur. J.* **2013**, *19*, 7895–7903.
46. Da Cunha, T.T.; Jung, J.; Boulon, M.-E.; Campo, G.; Pointillart, F.; Pereira, C.L.M.; Le Guennic, B.; Cador, O.; Bernot, K.; Pineider, F.; *et al*. Magnetic poles determinations and robustness of memory effect upon solubilization in a Dy-III-based single ion magnet. *J. Am. Chem. Soc.* **2013**, *135*, 16332–16335.
47. Pointillart, F.; Golhen, S.; Cador, O.; Ouahab, L. Slow magnetic relaxation in a redox-active tetrathiafulvalene-based ferromagnetic dysprosium complex. *Eur. J. Inorg. Chem.* **2014**, *2014*, 4558–4563.
48. Gao, F.; Zhang, X.-M.; Cui, L.; Deng, K.; Zeng, Q.-D.; Zuo, J.-L. Tetrathiafulvalene-supported triple-decker phthalocyaninato dysprosium(III) complex: Synthesis, properties and surface assembly. *Sci. Rep.* **2014**, *4*, 5928, doi:10.1038/srep05928.
49. Pointillart, F.; Bernot, K.; Golhen, S.; le Guennic, B.; Guizouarn, T.; Ouahab, L.; Cador, O. Magnetic memory in an isotopically enriched and magnetically isolated mononuclear dysprosium complex. *Angew. Chem. Int. Ed.* **2015**, *54*, 1504–1507.
50. Pointillart, F.; Jung, J.; Berraud-Pache, R.; le Guennic, B.; Dorcet, V.; Golhen, S.; Cador, O.; Maury, O.; Guyot, Y.; Decurtins, S.; *et al*. Luminescence and single-molecule magnet behavior in lanthanide complexes involving a tetrathiafulvalene-fused dipyridophenazine ligand. *Inorg. Chem.* **2015**, *54*, 5384–5397.

51. Feng, M.; Pointillart, F.; Lefeuvre, B.; Dorcet, V.; Golhen, S.; Cador, O.; Ouahab, L. Multiple single-molecule magnet behaviors in dysprosium dinuclear complexes involving a multiple functionalized tetrathiafulvalene-based ligand. *Inorg. Chem.* **2015**, *54*, 4021–4028.
52. Faulkner, S.; Burton-Pye, B.P.; Khan, T.; Martin, L.R.; Wray, S.D.; Skabara, P.J. Interaction between tetrathiafulvalene carboxylic acid and ytterbium DO3A: Solution state self-assembly of a ternary complex which is luminescent in the near IR. *Chem. Commun.* **2002**, 1668–1669, doi:10.1039/B204218E.
53. Pope, S.J.A.; Burton-Pye, B.P.; Berridge, R.; Khan, T.; Skabara, P.; Faulkner, S. Self-assembly of luminescent ternary complexes between seven-coordinate lanthanide(III) complexes and chromophore bearing carboxylates and phosphonates. *Dalton Trans.* **2006**, 2907–2912, doi:10.1039/B600598E.
54. Pointillart, F.; le Guennic, B.; Golhen, S.; Cador, O.; Maury, O.; Ouahab. L. High nuclearity complexes of lanthanide involving tetrathiafulvalene ligands: Structural, magnetic, and photophysical properties. *Inorg. Chem.* **2013**, *52*, 1610–1620.
55. Ran, Y.-F.; Steinmann, M.; Sigrist, M.; Liu, S.-X.; Hauser, J.; Decurtins, S. Tetrathiafulvalene-based lanthanide coordination complexes: Synthesis, crystal structure, optical and electrochemical characterization. *C. R. Chim.* **2012**, *15*, 838–844.
56. Feng, M.; Pointillart, F.; le Guennic, B.; Lefeuvre, B.; Golhen, S.; Cador, O.; Maury, O.; Ouahab, L. Unprecedented sensitization of visible and near-infrared lanthanide luminescence by using a tetrathiafulvalene-based chromophore. *Chem. Asian J.* **2014**, *9*, 2814–2825.
57. Pointillart, F.; le Guennic, B.; Cauchy, T.; Golhen, S.; Cador, O.; Maury, O.; Ouahab, L. A series of tetrathiafulvalene-based lanthanide complexes displaying either single molecule magnet or luminescence-direct magnetic and photo-physical correlations in the ytterbium analogue. *Inorg. Chem.* **2013**, *52*, 5978–5990.
58. Soussi, K.; Jung, J.; Pointillart, F.; le Guennic, B.; Lefeuvre, B.; Golhen, S.; Cador, O.; Guyot, Y.; Maury, O.; Ouahab, L. Magnetic and photo-physical investigations into Dy^{III} and Yb^{III} complexes involving tetrathiafulvalene ligand. *Inorg. Chem. Front.* **2015**, *2*, 1105–1117.
59. Simonsen, B.; Svenstrup, N.; Lau, J.; Simonsen, O.; Mork, P.; Kristensen, G.J.; Becher, J. Sequential functionalisation of bis-protected tetrathiafulvalene-dithiolates. *Synthesis* **1996**, *3*, 407–418.
60. Lin, H.-H.; Yan, Z.-M.; Dai, J.; Zhang, D.-Q.; Zuo, J.-L.; Zhu, Q.-Y.; Jia, D.-X. A water-soluble derivative of tetrathiafulvalene exhibiting pH sensitive redox properties. *New J. Chem*. **2005**, *29*, 509–513.
61. Llunell, M.; Casanova, D.; Cirera, J.; Bofill, J.M.; Alemany, P.; Alvarez, S. *SHAPE*; Version 2.1; Universitat de Barcelona*:* Barcelona, Spain, 2013.
62. Cosquer, G.; Pointillart, F.; le Guennic, B.; le Gal, Y.; Golhen, S.; Cador, O.; Ouahab, L. 3d4f heterobimetallic dinuclear and tetranuclear complexes involving tetrathiafulvalene as ligands: X-ray structures and magnetic and photophysical investigations. *Inorg. Chem.* **2012**, *51*, 8488–8501.
63. Pointillart, F.; Cauchy, T.; Maury, O.; le Gal, Y.; Golhen, S.; Cador, O.; Ouahab, L. Tetrathiafulvalene-amido-2-pyridine-*N*-oxide as efficient charge-transfer antenna ligand for the sensitization of Yb^{III} luminescence in a series of lanthanide paramagnetic coordination complexes. *Chem. Eur. J.* **2010**, *16*, 11926–11941.

64. Pointillart, F.; le Guennic, B.; Golhen, S.; Cador, O.; Maury, O.; Ouahab, L. A redox-active luminescent ytterbium based single molecule magnet. *Chem. Commun.* **2013**, *49*, 615–617.
65. Gonçalves Silva, F.R.; Malta, O.L.; Reinhard, C.; Güdel, H.U.; Piguet, C.; Moser, J.; Bünzli, J.C.G. Visible and near-infrared luminescence of lanthnaide-containing dimetallic triple-stranded helicates: Energy transfer mechanisms in the Sm^{III} and Yb^{III} molecular edifices. *J. Phys. Chem. A* **2002**, *106*, 1670–1677.
66. Lapadula, G.; Bourdolle, A.; Allouche, F.; Conley, M.; del Rosa, I.; Maron, L.; Lukens, W.W.; Guyot, Y.; Andraud, C.; Brasselet, S.; *et al*. Near-IR two photon microscopy imaging of silica nanoparticles functionalized with isolated sensitized Yb(III) centers. *Chem. Mater*. **2014**, *26*, 1062–1073.
67. Kahn, O. *Molecular Magnetism*; VCH: Weinhem, Germany, 1993.
68. Orbach, R. Spin-lattice relaxation in rare-earth salts. *Proc. R. Soc. Lond. A* **1961**, *264*, 458–484.
69. Rudowicz, C. Transformation relations for the conventional O_k^q and normalised $O'_k{}^q$ Stevens operator equivalents with $k = 1$ to 6 and $-k \leq q \leq k$. *J. Phys. C Solid State Phys.* **1985**, *18*, 1415–1430.
70. Görlder-Walrand, C.; Binnemans, K. Rationalization of Crystal-Field Parametrization. In *Hanbook on the Physics and Chemistry of Rare Earths*; Elsevier: Philadelphia, PA, USA, 1996; Volume 23, pp. 121–283.
71. Richardson, M.F.; Wagner, W.F.; Sands, D.E. Rare-earth trishexafluoroacetylacetonates and related compounds. *J. Inorg. Nucl. Chem.* **1968**, *30*, 1275–1289.
72. Binet, L.; Fabre, J.M.; Montginoul, C.; Simonsen, K.B.; Becher, J. Preparation and chemistry of new unsymmetrically substituted tetrachalcogenofulvalenes bearing $CN(CH_2)_2X$ and $HO(CH_2)_2X$ groups (X = S or Se). *J. Chem. Soc. Perkin Trans. 1* **1996**, 783–788, doi:10.1039/P19960000783.
73. Polasek, M.; Sedinova, M.; Kotek, J.; Vander Elst, L.; Muller, N.R.; Hermann, P.; Lukes, I. Pyridine-*N*-oxide analogues of DOTA and their gadolinium(III) complexes endowed with a fast water exchange on the square-antiprismatic isomer. *Inorg. Chem.* **2009**, *48*, 455–465.
74. Sheldrick, G.M. *SHELX97—Programs for Crystal Structure Analysis (Release 97-2)*; Tammanstrasse 4, D-3400; Institüt für Anorganische Chemie der Universität: Göttingen, Germany, 1998.
75. Altomare, A.; Burla, M.C.; Camalli, M.; Cascarano, G.L.; Giacovazzo, C.; Guagliardi, A.; Moliterni, A.G.G.; Polidori, G.; Spagna, R. *SIR97*: A new tool for crystal structure determination and refinement. *J. Appl. Cryst.* **1999**, *32*, 115–119.
76. Frisch, M.J.; Trucks, G.W.; Schlegel, H.B.; Scuseria, G.E.; Robb, M.A.; Cheeseman, J.R.; Scalmani, G.; Barone, V.; Mennucci, B.; Petersson, G.A.; *et al*. *Gaussian 09*, *Revision A.02*; Gaussian Inc.: Wallingford, CT, USA, 2009.
77. Perdew, J.P.; Burke, K.; Ernzerhof, M. Generalized gradient approximation made simple. *Phys. Rev. Lett.* **1996**, *77*, 3865–3868.
78. Adamo, C.; Barone, V. Toward reliable density functional methods without adjustable parameters: The PBE0 model. *J. Chem. Phys.* **1999**, *110*, 6158–6170.
79. Dolg, M.; Stoll, H.; Preuss, H. A combination of quasirelativistic pseudopotential and ligand field calculations for lanthanoid compounds. *Theor. Chim. Acta* **1993**, *85*, 441–450.

80. Weigend, F.; Ahlrichs, R. Balanced basis sets of split valence, triple zeta valence and quadruple zeta valence quality for H to Rn: Design and assessment of accuracy. *Phys. Chem. Chem. Phys.* **2005**, *7*, 3297–3305.
81. Tomasi, J.; Mennucci, B.; Cammi, R. Quantum mechanical continuum solvation models. *Chem. Rev.* **2005**, *105*, 2999–3094.
82. Cossi, M.; Barone, V. Time-dependent density functional theory for molecules in liquid solutions. *J. Chem. Phys.* **2001**, *115*, 4708–4717.
83. Improta, R.; Barone, V.; Scalmani, G.; Frisch, M.J. A state-specific polarizable continuum model time dependent density functional theory method for excited state calculations in solution. *J. Chem. Phys.* **2006**, *125*, 054103, doi:10.1063/1.2222364.
84. Allouche, A.-R. Gabedit—A graphical user interface for computational chemistry softwares. *J. Comput. Chem.* **2011**, *32*, 174–182.